Surf Zone Wave Measurements from Lidar Scanners: Analysis of Non-hydrostatic Processes

Kévin Martins*; Philippe Bonneton; Arthur Mouragues

UMR 5805 EPOC - CNRS University of Bordeaux, Pessac, France

Paul M. Bayle; Chris E. Blenkinsopp

WEIR, University of Bath, Bath, UK

Hervé Michallet

UMR 5519 LEGI - CNRS Grenoble Alpes University, Grenoble, France

ABSTRACT

Lidar scanners provide the ability to directly measure the free surface of breaking waves, however it is generally necessary to mount the scanners above the water surface on a nearshore structure such as a jetty. Pressure sensors on the other hand are easy to deploy and remain the simplest alternative to collect field measurements of surf zone waves, the free surface being generally reconstructed from the linear transfer function. Recent studies have highlighted the limitations of this traditional approach to describe geometric properties of non-linear waves. In the surf zone, this issue remains largely overlooked, principally due to the absence of direct measurements of the free surface elevation. The present contribution addresses this gap by using data collected by collocated sub-surface pressure sensors and lidar during the DynaRev set of experiments, which were performed at the prototype scale. During these experiments, a 1:15 sandy beach was exposed to irregular waves for 20 hours, and reached a quasi-equilibrium state at the end of the test phase, exhibiting a bar-terrace profile. In the inner surf zone, errors between 10% and 40% are obtained on second and third-order wave parameters with the classic transfer function based on linear wave theory. Only a recently developed non-linear weakly dispersive reconstruction method is found to be capable of describing wave-by-wave parameters and thus the root-mean square wave height H_{rms} in the surf zone. This has important implications for the estimation of wave height distributions based on pressure data, which are illustrated here, and calls for a reanalysis of old datasets and reconsideration of hypotheses based on pressure transducer datasets.

INTRODUCTION

Knowledge of wave height distributions is critical in coastal engineering applications as they provide the basis for predicting the evolution of incident wave energy in numerical models (*e.g.*, see Battjes and Janssen 1978; Thornton and Guza 1983). For a train of irregular and narrow-banded waves propagating in deep water (considered as a Gaussian process), Longuet-Higgins showed that the wave height of individual waves followed a Rayleigh distribution. A consequence is that the root-mean square value of the wave height distribution H_{rms} and $\sqrt{8\langle\zeta^2\rangle}$ are equal, $\sqrt{\langle\zeta^2\rangle}$ being the variance of the free surface elevation ζ. A number of studies have found that the Rayleigh distribution tends to overpredict the number of large waves (*e.g.*, see Forristall 1978). It was hypothesised that this behaviour was caused by wave non-linearities and partial wave breaking. However, Thornton and Guza (1983) showed that surf zone waves followed a Rayleigh distribution using surface elevation data collected by wave staffs. For decades, these results were unchallenged, although a number of studies have demonstrated that H_{rms} and $\sqrt{8\langle\zeta^2\rangle}$ considerably deviate from each other when wave non-linearities are important (Basco and Yamashita 1986; Michallet et al. 2011). This would explain why waves were mostly not found to be Rayleigh-distributed in the surf zone in recent studies by Power et al. (2016) and Stringari and Power (2019).

To date, the primary approach for collecting surf zone wave height measurements in the field has employed bottom-mounted pressure sensors combined with the classic transfer function method to retrieve the free surface elevation (*e.g.*, see Bishop and Donelan 1987). This approach needs a cutoff frequency to be applied to the high frequency part of the spectrum because of wave non-linearities (Bonneton and Lannes 2017). As a consequence, despite giving relatively accurate values for the elevation vari-

* *Corresponding author*: K. Martins, kevin.martins@u-bordeaux.fr

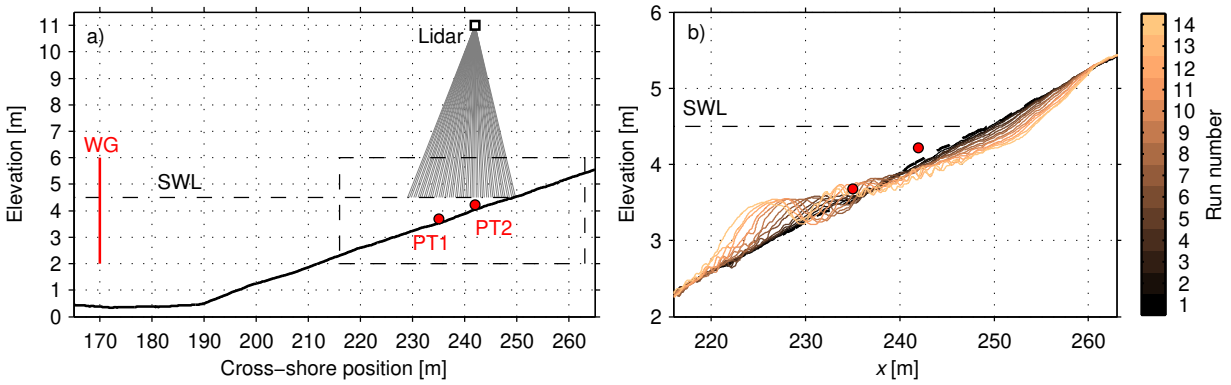

FIG. 1. Experimental setup (panel a) and evolution of the beach profile during Phase SB0 (panel b, 14 runs in total). The dashed rectangle in panel a corresponds to the flume region displayed in panel b. 'WG' refers to the wave gauge located at $x = 170$ m, which measured offshore wave conditions.

ance, this approach poorly describes the wave shape and individual wave height which makes the wave-by-wave analysis on surf zone datasets not appropriate (Martins et al. 2017a; Bonneton et al. 2018; Mouragues et al. 2019; Martins et al. 2020). Alternatives include the non-linear weakly dispersive reconstruction formula developed by Bonneton et al. (2018) or direct measurements with lidar technology (*e.g.*, see Martins et al. 2017b). Considering this, the objectives of the present contribution are to verify the findings of Martins et al. (2020) and extend their analysis to the wave-by-wave scale, using a new dataset which is particularly suited for this purpose (no tides). In particular, the effect of the method used to reconstruct the surface elevation from pressure on the estimation of wave height distributions is analysed.

METHODS

This study uses lidar and pressure data collected during the DynaRev set of experiments, which had the objective to assess the performance of a dynamic cobble berm revetment to tackle beach erosion and capture the underlying physical processes (Blenkinsopp et al. 2019). In this section, the experimental setup and the data processing methods are described.

Experimental setup and dataset

A series of experiments were performed at the prototype scale in the Large Wave Flume (Großer Wellenkanal, GWK) in Hannover, Germany. This contribution focuses on the SB0 phase ('Sandy Beach'), during which an initially 1:15 sandy beach ($D_{50} = 0.33$ mm) was exposed to irregular waves for 20 hours, with cycles of 2 hours in the wave forcing (JONSWAP spectrum characterized by a significant wave height $H_{m0} = 0.8$ m and a peak period $T_p = 6$ s). A total of 14 runs were performed, with durations increasing from 20 to 180 minutes, and the beach gradually adjusted to a bar-terrace equilibrium profile towards the end of these runs, see Figure 1b.

Following the approach of Martins et al. (2017b), three SICK LMS511 2D lidars were deployed approximately 7.3 m above the Still Water Level (SWL) to monitor wave transformation processes in the surf and swash zones. The scanners provided direct measurements of the free surface at high spatial and temporal resolution over a region extending from the outer surf zone (where the first waves were breaking) to the swash zone. The two pressure transducers (PT) used here correspond to those deployed at $x = 235$ and 242 m (Figure 1a). As the middle lidar scanner covered a region wide enough to capture the surface elevation at the two PT locations, only the data from this scanner is used here. Initially, the PTs were deployed at approximately 0.15 m from the seabed, but the distance to the seabed evolved with the runs as the beach adjusted to the wave forcing through time (Figure 1b). The distance between the sensors and the seabed was deduced from the beach profiles surveyed between each of the 14 runs. PTs and lidars were originally synchronized and recorded data at 25 Hz, but the data were re-sampled at 16 Hz and organized in 1024 second-long data bursts.

Reconstruction of the free surface elevation from pressure measurements

Three reconstruction formula are investigated here: the hydrostatic reconstruction, the classic transfer function based on linear wave theory (*e.g.*, see Bishop and Donelan 1987) and the weakly dispersive non-linear formula of Bonneton et al. (2018).

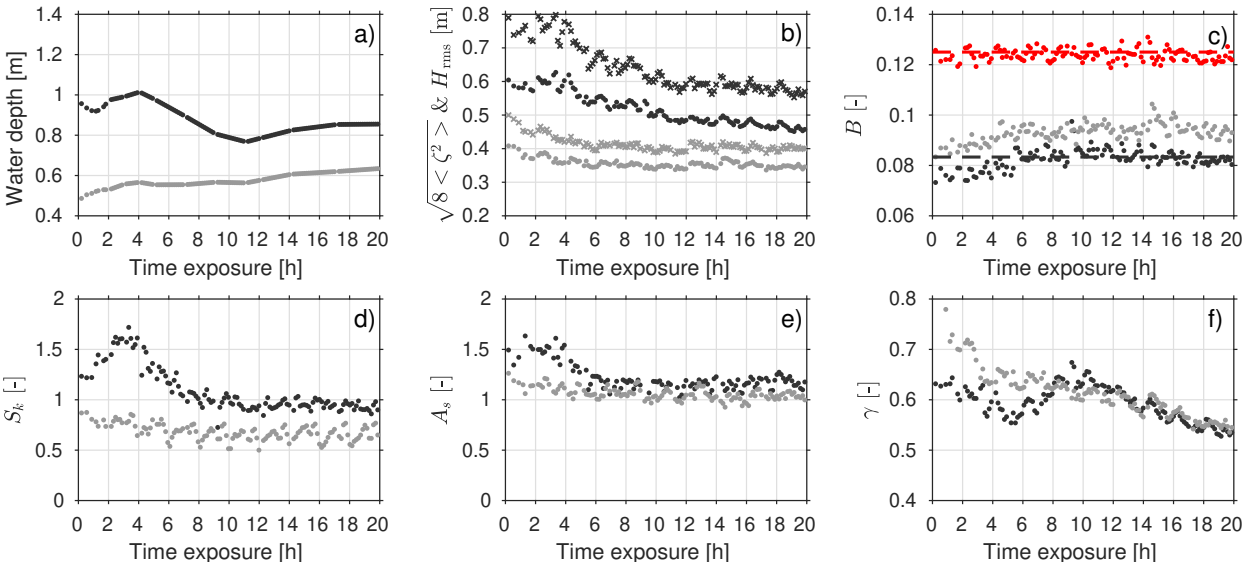

FIG. 2. Water depth (a) and wave parameters measured at PT1 (black dots) and PT2 (light gray dots) by the lidar scanner. Panel b) compares the root-mean square wave heights computed from the surface elevation variance (dots) with that from a wave-by-wave analysis (crosses). In panel c), the red dots corresponds to wave shape parameters B measured at the wave gauge located at $x = 170\,\mathrm{m}$. The red and gray dashed lines correspond to $B = 1/8$ and $1/12$ respectively. Panels d), e) and f) show the wave skewness, wave asymmetry and breaker index respectively.

These formulas are extensively described in references such as Bonneton et al. (2018) and Mouragues et al. (2019), and are only briefly summarised here.

The hydrostatic reconstruction of the free surface is obtained by neglecting the vertical acceleration in the momentum equation:

$$\zeta_{\mathrm{hyd}} = \frac{P_{\mathrm{m}} - P_{\mathrm{atm}}}{\rho g} + \delta_{\mathrm{m}} - h_0, \tag{1}$$

where P_{m} is the pressure measured at a distance δ_{m} from the bed, P_{atm} is the atmospheric pressure, ρ is the water density, g is the acceleration of gravity and h_0 is the mean water depth. The classic transfer method (hereafter TFM) applies a linear theory-based correction to the hydrostatic surface elevation Fourier transform, as follows:

$$\mathcal{F}\{\zeta_{\mathrm{lin}}\}(\omega) = K_{p,\mathrm{lin}}(\omega)\mathcal{F}\{\zeta_{\mathrm{hyd}}\}(\omega) \tag{2}$$

$$K_{p,\,\mathrm{lin}}(\omega) = \frac{\cosh(kh_0)}{\cosh(k\delta_m)} \tag{3}$$

$$\omega^2 = gk\tanh(kh_0), \tag{4}$$

where ω is the radial frequency and $\mathcal{F}$ is the Fourier transform. Bonneton et al. (2018) derived a non-linear formula for weakly dispersive waves which reads:

$$\zeta_{\mathrm{sl}} = \zeta_{\mathrm{hyd}} - \frac{h_0}{2g}\left(1 - \left(\frac{\delta_m}{h_0}\right)^2\right)\frac{\partial^2\zeta_{\mathrm{hyd}}}{\partial t^2} \tag{5}$$

$$\zeta_{\mathrm{snl}} = \zeta_{\mathrm{sl}} - \frac{1}{g}\left(\frac{\partial}{\partial t}\left(\zeta_{\mathrm{sl}}\frac{\partial\zeta_{\mathrm{sl}}}{\partial t}\right) - \left(\frac{\delta_m}{h_0}\right)^2\left(\frac{\partial\zeta_{\mathrm{sl}}}{\partial t}\right)^2\right) \tag{6}$$

This equation can be seen as an asymptotic shallow water approximation of the fully dispersive Bonneton-Lannes equation (Bonneton and Lannes 2017). However, for non-linear shallow water waves ($(kh)^2 \leq 0.3$) the weakly dispersive reconstruction of Eq. 6 (hereafter WDNL) gives better results than the fully dispersive one. Time derivatives are computed in the Fourier space. For the classic transfer function, a cutoff frequency of 0.42 Hz was used for both PTs (2.5 times the peak frequency, *e.g.*, see Thornton and Guza 1983). Cutoff frequencies ranging from 0.8 to 1.0 Hz were applied for the WDNL formula, following the recommendations of Martins et al. (2020).

RESULTS

Figure 2 displays the water depth (Figure 2a) and several wave parameters derived from the lidar data (Figure 2b-2f) at the location of the two PTs, as a function of the time exposure to the wave action. The evolution of the water depth during the SB0

phase reflects the beach morphological response to the wave action. At PT1, the local water depth first increases under the action of plunging waves right before that location (Figure 1b). As evidenced by the maximal values of surface elevation variance (Figure 2b) and wave skewness and asymmetry (Figures 2d and 2e), wave breaking was intense and frequent at this location within the flume between the 2nd and 4th hour of running time. The consistent generation of wave breaking-induced splashes right before PT1 could lead to a slight overestimation of the surface elevation variance at PT1 as detected by the lidar. A second phase is evident from the 4th to 11th hour of tests, which corresponds to the development of a bar/trough system. After this, the bar and the terrace extent progressed seaward, and the local water depth reached an equilibrium value towards the end of the runs. At PT2, the water depth gradually increased as the beach terrace developed.

The high degree of non-linearity present at the location of the PTs can be seen in third-order parameters (Figures 2d and 2e) but can also be observed in Figure 2b in the differences between $\sqrt{\langle\zeta^2\rangle}$ and H_{rms}, the latter being computed using wave-by-wave analysis (*e.g.*, Martins et al. 2016). The wave shape parameter $B = \sqrt{\langle\zeta^2\rangle}/H_{rms}^2$, shown in Figure 2c, better characterizes these differences. Close to the mean breaking point (around PT1, see Figure 2c), B reaches its minimal value (Michallet et al. 2011). Landward of the breaking point, in the inner surf zone, B increases as conditions become saturated. As no filtering was applied to the surface elevation dataset (*i.e.* no high-pass filter), some energy contained in the infragravity band at PT2 explains the higher B values at PT2 compared to PT1 (see also Michallet et al. 2011). Most importantly, B values are significantly different from the offshore value of 0.125 (Figure 2c), here taken at the location of the wave gauge ($x = 170$ m) and where linear wave theory can be considered applicable (*i.e.* $B = 0.125$). These deviations also suggest that the wave heights are no longer Rayleigh-distributed in the surf zone.

While the relative position in the surf zone of PT1 changes through the Phase SB0 (*i.e.* passing from outer to inner surf zone), PT2 remains in the inner surf zone. Considering this, several interesting observations can be made from second and third-order wave parameters shown in Figure 2. Despite the local water depth increases throughout SB0 (Figure 2a), the surface elevation variance, skewness and asymmetry remain relatively constant after only 4 hours of wave action. This indicates that the local wave conditions are dictated by what happens seaward, around the bar, rather than the local water depth. Consequently, the breaker index exhibits a consistent decrease throughout Phase SB0 (Figure 2f), despite the offshore forcing, local wave height and beach slope remaining similar for the last 10 hours of wave exposure (not shown here).

DISCUSSION

Close to the breaking point, Martins et al. (2017a), Bonneton et al. (2018) and, more recently, Mouragues et al. (2019) demonstrated that wave crest maximal elevations are consistently underestimated with the hydrostatic reconstruction or the TFM, based on linear wave theory.

Using field data collected using collocated PTs and lidars, Martins et al. (2020) found a similar behaviour everywhere in the surf zone. Furthermore, in the inner surf zone, these authors noted that due to the cutoff frequency needed with the TFM, this method brings only marginal improvements for describing bulk and wave-by-wave parameters compared to the hydrostatic reconstruction. Nonetheless, linear wave theory is arguably the most widely used approach to reconstruct the free surface of wave fields from the shoaling region to the shoreline. The hypothesis that $B = 1/8$, *i.e.* a Rayleigh-distributed linear wave field, is often made in both numerical or experimental studies of surf zone hydrodynamics (*e.g.*, see Thornton and Guza 1983; Apotsos et al. 2007). Considering the non-linear character observed here in the inner surf zone (Figure 2c), it is interesting to further investigate these concepts by assessing the capacity of the three reconstruction methods to represent the wave shape parameter B, which has implications for wave height distributions.

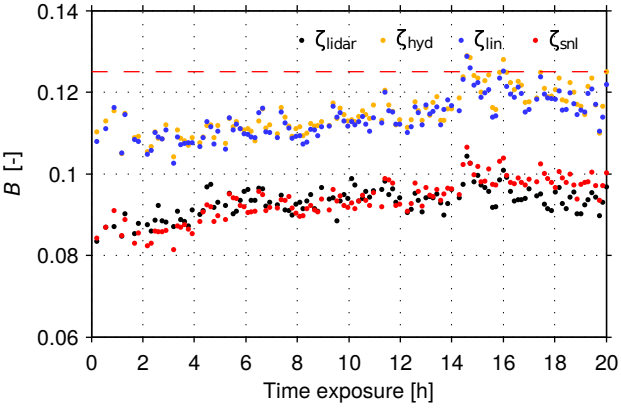

FIG. 3. Wave shape parameter B computed using the different reconstructed surface elevation signals and direct measurements from the lidar at PT2. The red dashed line corresponds to the 1/8 value.

At both PT locations, the errors on B with the hydrostatic reconstruction and the TFM is between 30% and 45% at PT1 (outer surf zone, not shown) and ranges between 25% and 30% at PT2 (inner surf zone, see Figure 3). The WDNL reconstruction derived in Bonneton et al. (2018) accurately represents B, with errors associated being less than 5%. The performance of the weakly dispersive non-linear reconstruction method to correctly represent B relies on the capacity of the method to correctly estimate $\sqrt{\langle\zeta^2\rangle}$ and H_{rms} (within 10% and 5% respectively for every burst presented here). By contrast, the reconstruction methods based on the hydrostatic hypothesis and the TFM underestimate H_{rms} by 20 to 30%. Towards the end of the phase (Figure 3), this almost leads to a 'linear wave' situation in the inner surf zone, with B approaching the 1/8 value, which is associated with linear waves propagating in intermediate to deep water. This point is particularly interesting as it highlights the paradoxal and cascading effects of the application of linear wave theory in the surf zone: if one assumes that linear wave theory can be applied in the surf zone (*i.e.* via the TFM), one would get comforted in his choice by this result, which suggests that non-linearities are weak.

To verify the effect of B errors made by the different reconstruction methods on surface elevation and wave height distributions, the results from the 3 hour-long SB0-13 and 14 runs are studied here in more detail. The comparison of the bulk parameters for the SB0-14 run (see Table 1) are consistent with the 1024 s-long data bursts presented above, and the results obtained by Martins et al. (2020). Figure 4a shows the wave height distribution computed for approximately 4050 waves from the wave gauge data ($x = 170$ m, Figure 1a) against the theoretical Rayleigh distribution. This comparison is consistent with the results presented earlier on B values at $x = 170$ m (Figure 2c), which suggests that linear wave theory applies, and waves are Rayleigh-distributed in 4-m depth. The wave height distributions computed on the lidar and PT2 with different reconstruction methods show a different picture (Figure 4b). The distributions computed using the signals reconstructed with the hydrostatic hypothesis or the TFM largely underestimate the number of waves with heights between 0.4 and 0.6 m, and thus completely miss the distribution tail and wave height extrema. Consistent with B values relatively far from 0.125 (Table 1), the measured wave height distributions are quite different from the theoretical Rayleigh distribution. The latter overestimates both ends of the distribution (large and small waves) and underestimates the number of waves with heights around H_{rms}. In contrast, a Weibull distribution with a shape factor $\kappa = 5$ gives a much better prediction of the measured wave height distribution in the inner surf zone, confirming the findings of Stringari and Power (2019), although they were obtained with the TFM.

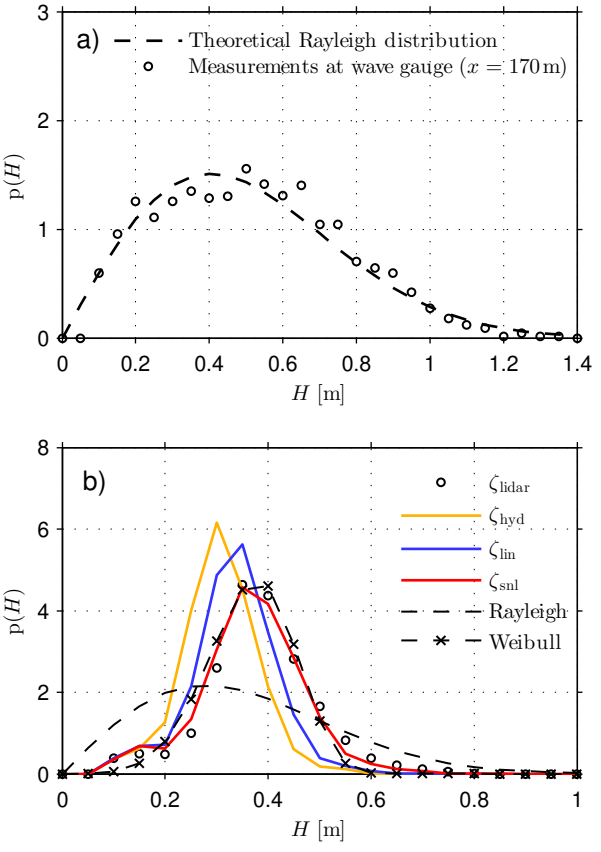

FIG. 4. Wave height distributions at the wave gauge ($x = 170$ m, panel a) and at PT2 (panel b), computed on the different reconstructed surface elevation signals.

CONCLUSIONS

This study uses new lidar and sub-surface pressure datasets collected in the lab at the prototype scale to extend the analysis of Martins et al. (2020) at the wave-by-wave scale. The errors on second and third-order wave parameters obtained for this new dataset with three surface elevation reconstruction methods are consistent with those obtained in the field by Martins et al. (2020). The wave-by-wave analysis presented herein further demonstrates and quantifies the errors on wave parameters such as the wave shape factor B, which are associated with non-hydrostatic and non-linear effects under breaking and broken

waves. As opposed to the hydrostatic reconstruction and the classic transfer function, the non-linear weakly dispersive method of Bonneton et al. (2018) accurately predicts the distribution of wave heights, its tail and thus wave extrema in the surf zone. Overall, the results presented here and in the references cited call for a revisit of old and unquestioned hypotheses, such as on the distribution of wave height in the surf zone. Technology such as lidar, which allow for direct measurements of the free surface, or the non-linear weakly dispersive reconstruction formula should help in this regard.

TABLE 1. Bulk parameters computed using the different surface elevation signals for the SB0-14 run.

Quantity	Lidar	Hydrostatic	TFM	WDNL
$\sqrt{8\langle\zeta^2\rangle}$ [m]	0.345	0.310	0.325	0.336
$\sqrt{8\langle\zeta^2\rangle}$ - error	-	19.4%	11.2%	5.1%
S_k	0.654	0.391	0.414	0.712
S_k - error	-	40.2%	36.7%	8.9%
A_s	1.034	0.738	0.820	0.921
A_s - error	-	28.6%	20.6%	10.9%
H_{rms} [m]	0.392	0.312	0.339	0.372
H_{rms} - error	-	20.3%	13.4%	4.9%
B	0.097	0.123	0.115	0.102
B - error	-	26.9%	18.3%	4.7%

ACKNOWLEDGMENTS

K. Martins greatly acknowledges the financial support from the University of Bordeaux, through an International Postdoctoral Grant (Idex, nb. 1024R-5030). The Ph.D. thesis work of A. Mouragues is cofunded by a DGA - Région Nouvelle-Aquitaine scholarship. The DynaRev project has received funding from the European Union's Horizon 2020 research and innovation programme under grant agreement No 654110, HYDRALAB+.

LITERATURE CITED

Apotsos, A., B. Raubenheimer, S. Elgar, R. T. Guza, and J. A. Smith, 2007: Effects of wave rollers and bottom stress on wave setup. *Journal of Geophysical Research: Oceans*, **112 (C2)**, doi:10.1029/2006JC003549.

Basco, D., and T. Yamashita, 1986: Toward a simple model of the wave breaking transition region in the surf zones. *Proceedings of the 20th Conference on Coastal Engineering, Taipei, Taiwan*, 955 – 970.

Battjes, J. A., and J. P. F. M. Janssen, 1978: Energy loss and set-up due to breaking of random waves. *Proceedings of the 16th Conference on Coastal Engineering, Hamburg, Germany*, 569 – 587.

Bishop, C. T., and M. A. Donelan, 1987: Measuring waves with pressure transducers. *Coastal Engineering*, **11 (4)**, 309 – 328, doi:10.1016/0378-3839(87)90031-7.

Blenkinsopp, C. E., and Coauthors, 2019: Dynamic coastal protection: resilience of dynamic revetments (DYNAREV). *Hydralab+ joint user meeting*, 129 – 139.

Bonneton, P., and D. Lannes, 2017: Recovering water wave elevation from pressure measurements. *Journal of Fluid Mechanics*, **833**, 399 – 429, doi:10.1017/jfm.2017.666.

Bonneton, P., D. Lannes, K. Martins, and H. Michallet, 2018: A nonlinear weakly dispersive method for recovering the elevation of irrotational surface waves from pressure measurements. *Coastal Engineering*, **138**, 1 – 8, doi:10.1016/j.coastaleng.2018.04.005.

Forristall, G. Z., 1978: On the statistical distribution of wave heights in a storm. *Journal of Geophysical Research: Oceans*, **83 (C5)**, 2353 – 2358, doi:10.1029/JC083iC05p02353.

Martins, K., C. E. Blenkinsopp, R. Almar, and J. Zang, 2017a: The influence of swash-based reflection on surf zone hydrodynamics: a wave-by-wave approach. *Coastal Engineering*, **122**, 27 – 43, doi:10.1016/j.coastaleng.2017.01.006.

Martins, K., C. E. Blenkinsopp, H. E. Power, B. Bruder, J. A. Puleo, and E. W. J. Bergsma, 2017b: High-resolution monitoring of wave transformation in the surf zone using a LiDAR scanner array. *Coastal Engineering*, **128**, 37 – 43, doi:10.1016/j.coastaleng.2017.07.007.

Martins, K., C. E. Blenkinsopp, and J. Zang, 2016: Monitoring individual wave characteristics in the inner surf with a 2-dimensional laser scanner (LiDAR). *Journal of Sensors, 2016*, 1 – 11, doi:10.1155/2016/7965431.

Martins, K., P. Bonneton, A. Mouragues, and B. Castelle, 2020: Non-hydrostatic, non-linear processes in the surf zone. *Journal of Geophysical Research: Oceans*, **125 (2)**, e2019JC015 521, doi:10.1029/2019JC015521.

Michallet, H., R. Cienfuegos, E. Barthélemy, and F. Grasso, 2011: Kinematics of waves propagating and breaking on a barred beach. *European Journal of Mechanics - B/Fluids*, **30 (6)**, 624 – 634, doi:10.1016/j.euromechflu.2010.12.004.

Mouragues, A., P. Bonneton, D. Lannes, B. Castelle, and V. Marieu, 2019: Field data-based evaluation of methods for recovering surface wave elevation from pressure measurements. *Coastal Engineering*, **150**, 147 – 159, doi:10.1016/j.coastaleng.2019.04.006.

Power, H. E., P. Nielsen, M. G. Hughes, T. Aagaard, and T. E. Baldock, 2016: Wave Height Distributions in the Surf Zone on Natural Beaches. *Journal of Coastal Research*, **(75 (10075))**, 917 – 921, doi:10.2112/SI75-184.1.

Stringari, C. E., and H. E. Power, 2019: The fraction of broken waves in natural surf zones. *Journal of Geophysical Research: Oceans*, **124 (12)**, 9114 – 9140, doi:10.1029/2019JC015213.

Thornton, E. B., and R. T. Guza, 1983: Transformation of wave height distribution. *Journal of Geophysical Research: Oceans*, **88 (C10)**, 5925 – 5938, doi:10.1029/JC088iC10p05925.